Heliyon 10 (2024) e26352

Contents lists available at ScienceDirect

Heliyon

journal homepage: www.cell.com/heliyon

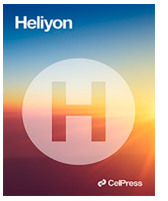

Research article

Determining mammalian cells state by fractal micromotion

Esteban Acerbo [a,c,d], Mariela I. Bellotti [a,b,d,e], Fabian J. Bonetto [a,b,c,d,*]

[a] Laboratorio de Cavitación y Tecnología, Centro Atómico Bariloche, San Carlos de Bariloche, R8402AGP, Argentina
[b] Comisión Nacional de Energía Atómica (CNEA), Centro Atómico Bariloche, San Carlos de Bariloche, R8402AGP, Argentina
[c] Consejo Nacional de Investigaciones Ciencia y Técnicas (CONICET), Buenos Aires, C1033AAJ, Argentina
[d] Universidad Nacional de Cuyo Instituto Balseiro, San Carlos de Bariloche, R8402AGP, Argentina
[e] Universidad Nacional de Río NegroSede Andina Carrera de Medicina, San Carlos de Bariloche, R8402AGP, Argentina

A B S T R A C T

We applied four fractal dimension estimation algorithms on the temporal electrical impedance signal of normal MDCK type II cell cultures monitored by ECIS technique and showed that the fractal dimension due to micromotion allows discriminating processes not sensed by the spectral impedance of the culture. In this work we subjected cell cultures to electric current damage and drug exposure to analyze the changes in the fractal structure of the temporal signal. Among the changes presented and detected are the differentiation between a healthy monolayer and one exposed to a drug, as well as the distinction between a seeding process and a wound-healing process performed by electric current. The four algorithms used were validated by applying them on topological functions of known fractal dimension, a study that determined the necessary conditions for a correct estimation.

1. Introduction

Benoît Mandelbrot created a formalism for a set of structures, ubiquitous in nature and in mathematics, which cannot be described by classical geometry in their completeness. These structures, as he defined them in 1982, are fractal structures, [1]. These occur naturally in the form of clouds, mountainous reliefs, dendrites and tree bark. Mandelbrot initially established that a structure is fractal by definition if its Hausdorff-Besicovitch dimension or fractal dimension exceeds the topological dimension, the latter being the classical geometrical dimension, represented by an integer. The dimension of an object is interpreted as the capacity of the structure to fill the space. For example, a plane presents a topological and fractal dimension equal to 2, since it fills the space in two directions, a solid body, like a sphere, presents both dimensions equal to 3. According to the definition of fractals, these do not fall into the category. Later, Mandelbrot redefined fractals simply as shapes composed of parts which are similar to the whole in some way, [2]. Despite these two definitions differ in rigor, they give an approximation to the complete definition of these complex forms. They also provide the necessary knowledge to carry out the objective of this work, which seeks to characterize the evolution of the electrical impedance of a microelectrode in the presence of a cell culture by its fractal behavior over time.

The fractal dimension for formally mathematical objects can be derived analytically, although this is not the case for real or physical phenomena with fractal properties. In these cases, the fractal dimension can be estimated from different algorithms. These are sensitive to experimental noise, number of measured data and range of fractal behavior, [3]. These problems lead to the definition of statistically fractal structures, shapes whose estimated fractal dimension fluctuates for different samples of the same class, [4]. This type of structures can be presented with fractal behavior in space (clouds, mountainous reliefs) or as a function of time (signals) and are characterized by the average value of the different independent estimates.

* Corresponding author. Laboratorio de Cavitación y Tecnología, Centro Atómico Bariloche, San Carlos de Bariloche, R8402AGP, Argentina.
E-mail address: fabian.bonetto@gmail.com (F.J. Bonetto).

https://doi.org/10.1016/j.heliyon.2024.e26352
Received 10 July 2023; Received in revised form 9 February 2024; Accepted 12 February 2024
Available online 24 February 2024

1.1. Electric cell-substrate impedance sensing technique

The *Electric Cell-Substrate Impedance Sensing* or ECIS technique is based on the non-invasive study of the spectral impedance of a cell culture grown on a biocompatible surface and immersed in culture medium, [5–8]. On the substrate, below the cells, is an array of microelectrodes which allow to monitor the electrical response of the system as a current flows between them. The presence of the cell culture modifies the impedance of the system, since it hinders the passage of the current. From the analysis of this change in spectral impedance of the system, it is possible to quantitatively evaluate the state of the cells and their properties [9,10], as well as to observe fluctuations due to the cell movement over the electrode, [11,12].

The basic instruments for the application of the ECIS technique consists of a wave generator, a lockin amplifier (LIA), a computer and a biocompatible substrate with integrated microelectrodes. In Fig. 1 a schematic of the measurement system is shown.

During the measurement process the wave generator *Hewlett-Packard* HP33120A applies a sinusoidal signal of 0.1 V_{rms} to the electrode through a load resistance of 100 $k\Omega$. In this way, an alternating current of less than 1 μA_{rms} is administered, which does not generate detectable changes in the cells, so it is noninvasive, [13]. The potential drop over the electrode is measured by means of a lock-in amplifier *Stanford Research Systems* SR530 connected in parallel. From this measurement, the amplitude and phase angle of the voltage are obtained, values that are later recorded in a computer. The excitation frequency is pre-determined by the user in the computer, allowing to set a number of frequencies to measure sequentially, measuring the impedance spectre.

The electrode used was the 96W1E electrode array obtained from Applied BioPhysics Inc. This consists of 96 independent wells, each with two 350 μm diameter microelectrodes as shown in Fig. 2. This arrangement of wells, together with the measurement system, allows the monitoring of up to 24 cell cultures simultaneously. Both the active microelectrode and the counter electrode are identical, and therefore the contribution of both to the electrical response of the system is going to be the same.

1.2. Cell culture procedures

Only the Madin Darby Canine Kidney type II (MDCKII or MDCK) cell line was used in this work. The cells are derived from healthy female Cocker Spaniel (*Canis familiaris*) kidney epithelium biopsies by S. Madin and N. Darby in 1958, [14]. These are considered good models of human cells, [15]. It has also been widely used in research associated with the ECIS technique and in previous work carried out by the working group, since it shows a high level of adhesion to the substrate on which it is seeded, [13,16]. This cell line comes from the ATCC (code PTA-6500), and was obtained through the Asociación Banco Argentino de Células (ABAC).

The cells were grown in sterile flasks (25 cm^2 Nalgene) and incubated at a fixed temperature of 37°C and in a controlled atmosphere with 80% humidity and 5% concentration of CO_2. These conditions were achieved inside an incubator which has an integrated temperature control system and a gas pumping system, which regulated the atmospheric concentration by calibrated flowmeters. Ambient humidity was achieved by depositing sterilized water on a tray inside the incubator and renewing its contents periodically.

The culture medium used was Dulbecco (DMEM F12, GIBCO) modified, supplemented with 10% of fetal bovine serum, which mainly provides proteins and supplements that favor cellular anchorage, 1% of antibiotic solution (penicillin, streptomycin, etc.), HEPES buffer and 1% of L-Glutamine. We adjusted the final pH of the medium to a value of 7.4 with sodium hydroxide or hydrochloric acid as appropriate, [17]. We changed the complete culture medium approximately twice a week.

When the cells reach 70% of the total surface area of the flask they are trypsinized, both for subculture purposes and for measuring from ECIS technique. Cell suspensions were obtained by the usual trypsinization procedure (0.05 *w/v* trypsin-EDTA 0.53 mM 4 *Na*). Prior to seeding on the microelectrodes, they are treated with the proteins present in the complete medium (serum), improving cell attachment. We then seeded them with 0.5 ml of suspension at a cell concentration of $10^4 - 10^5$ cells/*ml*.

1.3. Micromotion

The temporal evolution of the electrical impedance of covered microelectrodes presents small fluctuations of low amplitude and short duration when measured repeatedly. This phenomenon is due to the movement carried out by the cells on the substrate,

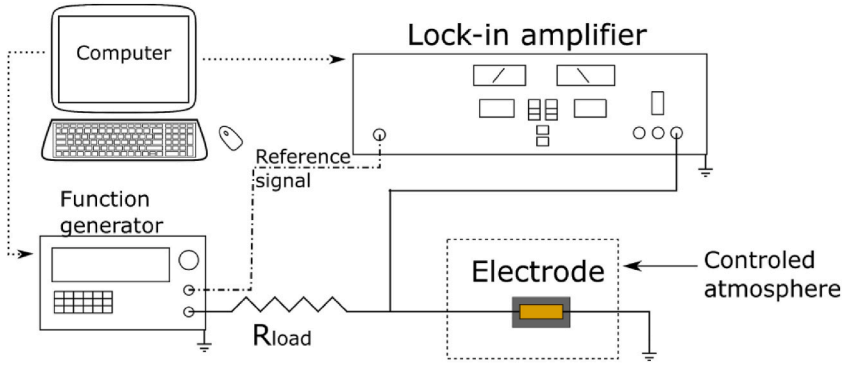

Fig. 1. Standard ECIS measurement arrangement.

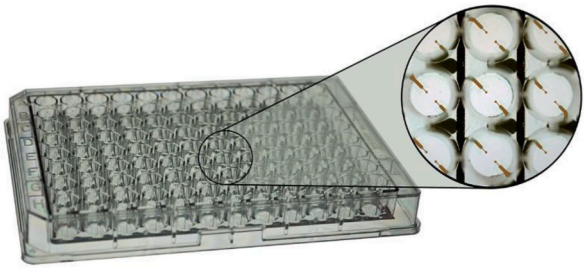

Fig. 2. Commercial electrode used in this work. This consists of a 12-row array of 8 independently culture wells. Inside each well there are two microelectrodes of 350 μm in diameter. The measurement system allows the monitoring of up to 20 cell cultures simultaneously. This image was obtained from "https://www.biophysics.com/culturewarе.php".

especially, variations in the height of the basement membrane above the electrode, in the strength of the intercellular junctions and in the geometry of spaces not occupied by cells. This movement, in previously published studies was observed by means of optical interference techniques and by the ECIS technique, in which it was determined that the fluctuations in the height at which the cells are found occurs at nanometric scales, thus obtaining the name micromotion or micromovement, [11,12,18]. Moreover, Lo et al. observed that cell movement can be related to the metabolic activity of these in the culture, therefore obtaining information of the movement can result in a recognition parameter of the nature of cells or their state, [19].

In this work we seek to obtain information of the cellular status by the fractal structure of the impedance signal due to micromotion. For this, we will use the ECIS technique, which allows us to obtain the temporal evolution of the system electrical impedance. By focusing in a single culture and exciting with a unique frequency the data acquisition rate increased dramatically, allowing to register fast fluctuations in the impedance signal, resulting in a measurement with temporal fractal structure.

2. Used algorithms

The calculation of the fractal dimension, especially of a signal, can be performed by several well-known algorithms although, through a literature review only four algorithms were selected for this work. The first being *Higuchi* 's algorithm [20], this one was devised to obtain a fast and stable estimate of the fractal dimension of a signal using little signal data, [21,22]. Moreover, two algorithms proposed by Raghavendra et al. [23] were used. One consists in a modification to the classical *box-counting* algorithm [2,24], for estimating the fractal dimension of a discretely sampled signal in time called *Multiresolution box-counting*. The second one considers the Euclidean distance between points of the signal instead of the number of boxes that fall between them, called the Multiresolution *Length-Based* algorithm. The last algorithm considered was proposed by Hurst when investigating water accumulation and discharge problems in lakes and rivers, this is the *Reescaled range* method. It is applicable to the analysis of the erratic behavior in time of temperature records, Brownian motion, discharge of water bodies and more, [25,26]. In this work, the same was used to analyze apparent resistance and capacitance records over time. This implementation was already performed by Giaever et al., [12]. This algorithm, like *Higuchi* 's, does not consider the sampling frequency or the temporal structure of the signal, and therefore, it is insensitive to the magnitude of the signal.

A known problem in the calculation of fractal dimensions on real structures is that their estimated dimension depends strongly on the algorithm used, [27–29]. This makes each estimate comparable with estimates made by the same algorithm. The algorithms also have different sensitivities to the fractal dimension to be estimated, ideally an algorithm correctly estimates the fractal dimension of the signal for the entire range [1,2]. On the other hand the sampling frequency of the signal can influence the estimation of the fractal

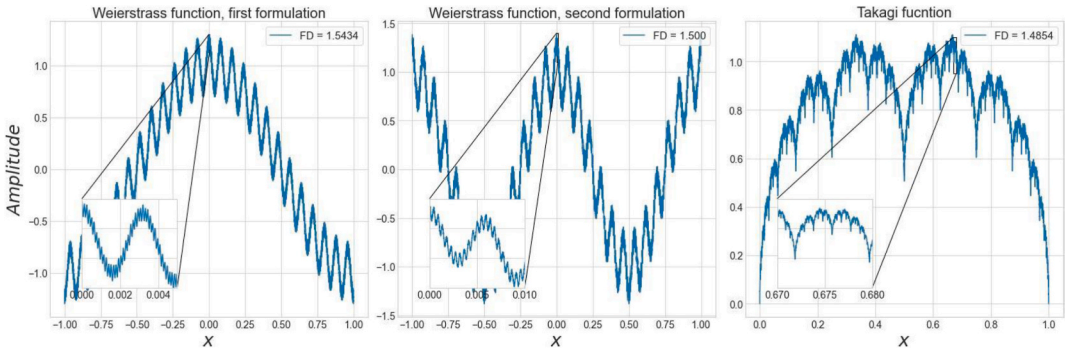

Fig. 3. Topological functions with known fractal dimension (FD) used for the study of fractal dimension estimation algorithms on discrete signals. **Left**: Weierstrass cosine function first formulation. **Center**: Weierstrass cosine function second formulation. **Right**: Takagi function. Each figure includes an increase of the graph on the abscissa axis showing a self-similar structure characteristic of fractal structures.

dimension, as well as the number of points that is necessary to perform a good estimation.

Therefore, in a first instance, these algorithms were verified with respect to topological functions with known fractal dimension and from this study the necessary conditions for a correct estimation of fractal dimension were determined. Two topological functions were considered, the Weierstrass cosine function, of which two formulations were used, and the Takagi function. Both functions are topological since they are continuous at all points but derivable at none and also present known fractal structure. These three curves are shown in Fig. 3. On each of the curves a magnification over the scale of the abscissae is performed to observe the self-similar behavior in scale.

The algorithms were implemented in Python language code. The code for *Higuchi*, the *Multiresolution box-counting* and *Multiresolution Length-Based* algorithms was programmed by the author of this work, while the code for the *Reescaled range* algorithm was obtained from the repository of Dmitry Mottl, [30].

3. Results

Knowing the conditions to be met by the signal for the algorithms to correctly estimate the fractal dimension, they will be applied on the experimental impedance signal of a culture well's microelectrode-array (MEA) in absence and presence of a cell culture. Two independent experiments were performed where the cell culture was exposed to different conditions. This was done in order to estimate the fractal dimension in them and to observe if it provides information of the cell culture. Before showing the results of the experiments, we will detail the steps performed on the signal before estimating the fractal dimension.

First, the MEA monitoring is performed using the experimental setup detailed in Fig. 1, where a single microelectrode was excited with a sinusoidal function of 100 mV amplitude and fixed excitation frequency. The frequencies used are 1000 Hz or 64,000 Hz, which are going to be denoted as LF and HF for low and high excitation frequency, respectively. By fixing the monitored microelectrode and the excitation frequency, the system achieves a data acquisition period of $\Delta t = 0.28\ s$ at low excitation frequency or LF and $\Delta t = 0.15\ s$ at high excitation frequency or HF. For this measurement configuration the lock-in amplifier time constant used is 0.3 s.

In Fig. 4 is shown the resistance and capacitance evolution resulting from monitoring a confluent culture. In the subfigure on the left, corresponding to the evolution of the resistance, we observe close-ups on the signal at different temporal resolutions. From this, it can be seen that the signal presents a self-similar structure at different amplitudes, characteristic of a fractal structure. It is also observed the frequency of data acquisition for resolutions close to seconds, being this the lower limit of fractal behavior. On the other hand, before estimating the fractal dimension of the measured signal, it was segmented in equal parts, each one with a quantity between 9000 and 10,000 points, which are enough for a correct estimation. Simultaneously, the amplitude of the signal was normalized so that the average step Δy is greater than $3\ 10^4\ \Delta t$. This provides the conditions for the correct estimation of the *Multiresolution* algorithms.

All segments were treated as independent signals, thus estimating the fractal dimension of each one. In this way, a statistical estimate of the fractal dimension is obtained for a culture in a given state, be it confluent, in the process of seeding or during a wounding and healing assay. Representative to all algorithms, Fig. 5 shows the power laws, in double logarithmic scale, resulting from applying the *Multiresolution Length-based* algorithm on each segment of Fig. 4 resistance and capacitance signal. The legend of the figure indicates that the estimated fractal dimension of each segment presents distinguishable values for the same cell state, showing that the uncertainty due to the linear fit underestimates the real one. That is why we will consider as fractal dimension value the average of the different segments, together with the deviation they present.

Tables 1 and 2 show the statistical fractal estimation values of the resistance and capacitance signals respectively, for every culture state measured and considered in this work. The first column of the tables describes the cell status, the second column indicates the frequency of excitation used to excite the MEA, the rest of the columns shows the fractal dimension estimation algorithm used for that value.

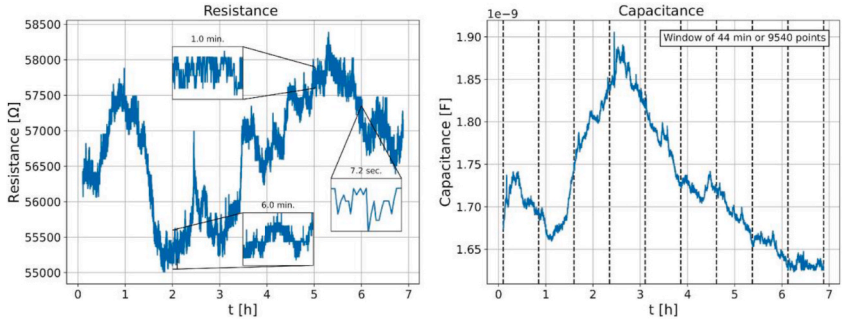

Fig. 4. Evolution of the apparent resistance and capacitance of a confluent culture. In the resistance subfigure (**left**), different increases in time resolution are shown, where the self-similarity of the signal at different signal amplitudes can be appreciated. Also observed for resolutions of the order of seconds is the frequency of data acquisition, this being the lower limit of the fractal behavior. In the capacitance subfigure (**right**) the way the signal was segmented for the statistical estimation of the fractal dimension is shown.

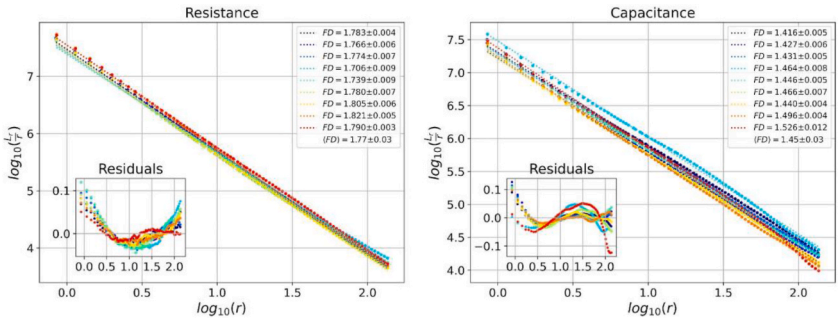

Fig. 5. Power law obtained by applying the *Multiresolution Length-based* algorithm on the resistance (**left**) and capacitance (**right**) signal segmented in 9500 point intervals. The fractal dimension of each segment was estimated by means of the power law.

Table 1
Resistance over time signal fractal dimension estimation table for different culture states. The culture states contemplated in this work includes a bare electrode (no culture), an electrode during the culture seeding process, a confluent culture, a culture during electrical wounding and healing assay and, lastly, a pharmacological death assay. The frequencies used to measure the impedance signals were 1000 Hz or 64,000 Hz, denoted as LF and HF respectively in the second column. It is also shown the algorithm used to estimate the fractal dimension in the later columns.

Cell Status	Freq.	HI.	MR. BC.	MR. LB	RS.
Bare electrode A	LF	1.997 ± 0.001	2.012 ± 0.002	2.012 ± 0.002	1.72 ± 0.03
Bare electrode A	HF	2.000 ± 0.001	2.009 ± 0.001	2.001 ± 0.001	1.84 ± 0.02
Bare electrode B	LF	1.999 ± 0.001	2.012 ± 0.001	2.012 ± 0.001	1.75 ± 0.03
Seeding process	LF	1.57 ± 0.13	1.67 ± 0.11	1.67 ± 0.11	1.72 ± 0.02
Confluent culture	LF	1.76 ± 0.05	1.77 ± 0.04	1.77 ± 0.04	1.65 ± 0.03
Confluent culture	HF	1.95 ± 0.03	1.97 ± 0.02	1.97 ± 0.02	1.61 ± 0.02
Wounded culture (healing)	LF	1.29 ± 0.12	1.43 ± 0.13	1.43 ± 0.13	1.70 ± 0.04
Healed confluence (Recently)	LF	1.68 ± 0.04	1.72 ± 0.03	1.72 ± 0.03	1.68 ± 0.03
Healed confluence (Post 24hs)	LF	1.48 ± 0.06	1.53 ± 0.06	1.53 ± 0.06	1.56 ± 0.04
Pharmacological assay	LF	1.56 ± 0.05	1.59 ± 0.05	1.59 ± 0.05	1.58 ± 0.04
Pharmacological assay	HF	1.71 ± 0.12	1.81 ± 0.09	1.81 ± 0.09	1.64 ± 0.04

Table 2
Capacitance over time signal fractal dimension estimation table for different culture states. The culture states contemplated in this work includes a bare electrode (no culture), an electrode during the culture seeding process, a confluent culture, a culture during electrical wounding and healing assay and, lastly, a pharmacological death assay. The frequencies used to measure the impedance signals were 1000 Hz or 64,000 Hz, denoted as LF and HF respectively in the second column. It is also shown the algorithm used to estimate the fractal dimension in the later columns.

Cell Status	Freq.	HI.	MR. BC.	MR. LB	RS.
Bare electrode A	LF	1.987 ± 0.001	2.007 ± 0.001	2.007 ± 0.001	1.79 ± 0.04
Bare electrode A	HF	1.998 ± 0.001	2.008 ± 0.001	2.008 ± 0.001	1.76 ± 0.02
Bare electrode B	LF	1.994 ± 0.001	2.009 ± 0.001	2.009 ± 0.001	1.75 ± 0.03
Seeding process	LF	1.51 ± 0.06	1.64 ± 0.04	1.64 ± 0.04	1.74 ± 0.02
Confluent culture	LF	1.46 ± 0.04	1.44 ± 0.03	1.44 ± 0.03	1.41 ± 0.04
Confluent culture	HF	1.92 ± 0.06	1.95 ± 0.05	1.95 ± 0.05	1.65 ± 0.02
Wounded culture (healing)	LF	1.31 ± 0.12	1.42 ± 0.13	1.42 ± 0.13	1.63 ± 0.08
Healed confluence (Recently)	LF	1.44 ± 0.05	1.40 ± 0.04	1.40 ± 0.04	1.39 ± 0.02
Healed confluence (Post 24hs)	LF	1.38 ± 0.04	1.37 ± 0.04	1.37 ± 0.04	1.39 ± 0.02
Pharmacological assay	LF	1.48 ± 0.04	1.46 ± 0.03	1.46 ± 0.03	1.45 ± 0.02
Pharmacological assay	HF	1.68 ± 0.05	1.80 ± 0.04	1.80 ± 0.04	1.68 ± 0.05

3.1. Bare electrodes

First, the fractal dimension was estimated for the signal corresponding to cell-free or bare microelectrodes. Since they are in contact only with the electrolyte, the culture medium, the fluctuations are due to the electronic noise present in the measuring equipment.

Two bare microelectrodes or MEA's monitored at 1000 Hz for a period of 15 min and only one of the two was excited at 64,000 Hz for 45 min. Since these monitors were for times shorter than those involved in measuring 9000 points no statistical analysis of the signals was performed.

In any case, a bare electrode does not exhibit long duration fluctuations such as those observed in Fig. 4, so it is not considered

necessary. The two MEA's used were denoted as MEA A and MEA B.

For the bare electrode fractal dimension the reported values of fractal dimension by the algorithms *Higuchi, Multiresolution Box-Counting* and *Multiresolution Length-based* coincide with the presence of electronic white noise in both high and low excitation frequencies. On the other hand, the *Reescaled Range* method underestimates the fractal dimension of the three signals. This was observed by analyzing the sensitivity of the algorithms as a function of the fractal dimension to be estimated with topological functions.

3.2. Normal culture

To characterize the fractal behavior of the normal MDCK type II cells, the fractal dimension was estimated during the seeding process and confluent state of the culture. The latter is determined at low and high excitation frequencies. The fractal dimension of resistance and capacitance as a function of time was estimated for each of these measurements.

The seeding process, being dynamic in time, presents a higher deviation than the other estimates. This is due to being an average of different coverage of the electrode by the cells, changing continuously the fractal dimension. Nevertheless, both impedance signals values differ from the bare electrode and, in the case of the capacitance, the value is different from that of the confluent monolayer by the *Multiresolution* and *Reescaled Range* algorithms.

On the other hand, the fractal dimension calculated of a healthy confluent culture presents a more steady value through time, as well as similar values reported for the resistance and capacitance by the four algorithms. In addition, different fractal behavior as a function of the applied excitation frequency was observed. At 64,000 Hz the estimation values tend to 2, as reported for bare electrodes. This could be caused by the change in the data acquisition rate, which becomes faster at higher excitation frequencies or due to greater influence of electronic noise compared to low frequencies.

3.3. Wound healing assay

As a first experiment we are going to report a wounding and healing assay on a normal MDCK type II confluent culture, experiment that has been performed repeatedly, so that the evolution is known. In order to see if the fractal behavior of the cell culture allows differentiation of the three stages of the assay, a MEA at low excitation frequency was monitored during all these stages. First, it was performed in the presence of the confluent culture, then after the wound by electric current and finally, when confluence was reached again by healing.

The wounding of the culture by electric current is performed by administering a potential of 5 V_{AC} at 40 kHz for 30s on the MEA of 350 μm diameter. This produces irreparable damage to the cell membrane resulting in death by necrosis of all cells above the microelectrodes. As the cells are killed, the impedance of the system is equivalent to bare and the healing process begins. In this instance the cells surrounding the microelectrode reproduce by occupying the space generated by the electric current and the culture reaches confluence once again, [31]. This evolution was monitored continuously, therefore, fractal estimation for the healing and newly confluent stage were made. Finally, the fractal dimension was monitored one day after healing.

During culture healing the estimated resistance fractal dimension is smaller and relative to the applied algorithm for the *Multiresolution* and *Higuchi* methods, compared to confluent culture estimates. It is notable, that after the electrical current, the spectral impedance is the same as the bare electrode, but this is not the case for the fractal dimension of the signal which differ significantly. Moreover, the fractal dimension estimation during the healing stage, does not coincide with the fractal dimension estimated for the seeding process. This may be because they are two different phenomena. In seeding, the cells in suspension adhere to the surface and to the microelectrode, subsequently duplicating themselves by filling the entire available surface until the confluent monolayer is formed. On the other hand, when wounding by electric current, the cells reproduce by filling the free space from the outside inwards. Note that the healing stage, as the seeding process, being a time-varying state of the culture, the different segments of the signal present a wider distribution of fractal dimensions, which is reflected in the increase of the deviation.

After confluence was reached again, by the algorithms *Higuchi, Multiresolution Box-Counting* and *Multiresolution Length-based*. Similar resistance fractal dimension values were obtained for both confluence states, either before the wound test or after healing. On the other hand, the estimations performed by applying the *Reescaled Range* algorithm do not differentiate the stages of the wound and healing test in fractal behavior.

Finally, the confluent monolayer was monitored one day after assay and culture healing, where there was a decrease in fractal dimension. A smaller fractal dimension implies less fluctuations due to cell micromotion, therefore, this may indicate a relaxation of the cell culture after healing in which the movement is decreased.

When performing the same analysis on the capacitance signal as a function of time, *Higuchi* and both *Multiresolution* algorithms showed no sensitivity to the different stages of the test, that is, the calculated values did not differ from each other. However, the *Reescaled Range* algorithm does discriminate between the different stages of the test. It is yet to understand how an algorithm is sensible to the different stages by processing one signal but not the other, and why this differs with the algorithm applied.

3.4. Pharmacological death assay

The second experiment performed to study the scope of the fractal behavior analysis of the impedance signal of a cell culture, was to induce cell death pharmacologically, [32]. It is known from experiments performed within the working group that the drug 1A-116 is able to kill normal MDCK type II cells in a time window longer than 24 hs. This would allow us to observe if the fractal behavior of the signal is modified. With this in mind, a MEA fractal behavior at confluence was monitored before and right after drug delivery at high

excitation frequency (HF). The fractal behavior of cell culture after drug administration at low excitation frequency (LF) was also analyzed for comparison.

Upon administration of the drug in the culture medium, the cells showed a decrease in both impedance signals fractal behavior at HF, and in the case of the resistance, also at LF. This is attributed to a reduction in cell micromotion by the drug presence, resulting in less signal fluctuations, reflected in a smaller fractal dimension. It should be noted that this change in fractal behavior was not observed by spectral impedance, both in resistance and capacitance, these spectra being equal to that of a healthy confluent monolayer.

By sensing a change in the fractal dimension values of the capacitance only at HF, it is indicating that the sensibility of the fractal analysis is dependable on the excitation frequency used. Although, no further exploration was made in this matter yet.

Using the *Reescaled range* algorithm, no drug delivery was sensed in the culture medium, estimating the same fractal dimension values as for a healthy confluent monolayer for both excitation frequencies.

4. Conclusions

The aim of focusing on fractal signal behavior due to cell micromotion is to obtain information on the state of the culture, which is not achieved by monitoring its spectral impedance. To analyze the scope of this tool in discrimination, two independent experiments were carried out, a wound and healing test and a pharmacological death test. In all cases, the fractal dimension of the impedance signal was estimated by four different algorithms, *Higuchi, Multiresolution Box-Counting, Multiresolution Length-based* and *Reescaled Range*. From the results obtained, it is possible to conclude that the fractal dimension is a valid measure to determine certain processes that the cell culture undergoes, complementing the information provided by the impedance spectra.

It is to be considered that not all algorithms are sensible to the same processes, and the sensitivity of the algorithms is dependent on the excitation frequency used. This results in each algorithm being comparative against estimates made by itself. Despite this, good repeatability was achieved between the *Higuchi* and both *Multiresolution* algorithms, but not with the estimates made with the *Reescaled range* method.

During these experiments a fractal characterization of healthy MDCK type II cells over two 350 μm identical microelectrodes was accomplished. It remains to be understood why the capacitance signal presents a fractal dimension value less than 1.5 (or Hurst exponent greater than 0.5), which would indicate a temporal persistence in its evolution. That is to say, that the fluctuations in the capacitance present a dependence of its state in previous times or that the cell or the cell culture as a whole has memory of its previous state. On the other hand, this behavior is not present in the resistance signal since it has a fractal dimension greater than 1.5. Nonetheless, these values are characteristic of the confluent cell state, this was verified by re-obtaining them after electrical wound healing.

Data availability statement

The data that support the findings of this study are available from the corresponding authors upon request.

CRediT authorship contribution statement

Esteban Acerbo: Writing – review & editing, Writing – original draft, Validation, Software, Project administration, Methodology, Investigation, Formal analysis, Data curation. **Mariela I. Bellotti:** Supervision, Resources, Project administration, Methodology, Investigation, Conceptualization. **Fabian J. Bonetto:** Supervision, Methodology, Investigation, Conceptualization.

Declaration of competing interest

The authors declare that they have no known competing financial interests or personal relationships that could have appeared to influence the work reported in this paper.

References

[1] Benoit B. Mandelbrot, The Fractal Geometry of Nature, vol. 1, WH Freeman, New York, 1982.
[2] Jens Feder, The Fractal Dimension, Springer, 1988, pp. 6–30.
[3] Joe Brewer, Larry Di Girolamo, Limitations of fractal dimension estimation algorithms with implications for cloud studies, in: Atmospheric Research, vol. 82, 2006, pp. 433–454, 1-2.
[4] J. Guyonnet, et al., in: Statistics of Roughness for Fluctuating Interfaces: A Survey of Different Scaling Analyses, 2019, p. 11726, *arXiv preprint arXiv:1904*.
[5] I. Giaever, C.R. Keese, Monitoring fibroblast behavior in tissue culture with an applied electric field, in: Proceedings of the National Academy of Sciences, 81.12, 1984, pp. 3761–3764.
[6] I. Giaever, C.R. Keese, Use of electric fields to monitor the dynamical aspect of cell behavior in tissue culture, in: IEEE Transactions on Biomedical Engineering, 33.2, 1986, pp. 242–247.
[7] I. Giaever, C.R. Keese, A morphological biosensor for mammalian cells, in: Nature, 366.6455, 1993, pp. 591–592.
[8] C.R. Keese, I. Giaever, A biosensor that monitors cell morphology with electrical fields, in: IEEE Engineering in Medicine and Biology Magazine, 13.3, 1994, pp. 402–408.
[9] Pierre O. Bagnaninchi, Nicola Drummond, Real-time label-free monitoring of adipose derived stem cell differentiation with electric cell substrate impedance sensing, in: Proceedings of the National Academy of Sciences, 108.16, 2011, pp. 6462–6467.
[10] Giana Fabián Eduardo, José Bonetto Fabián, In′es Bellotti Mariela, Assay based on electrical impedance spectroscopy to discriminate between normal and cancerous mammalian cells, in: Physical Review E, 97.3, 2018 032410.

[11] I. Giaever, C.R. Keese, Micromotion of mammalian cells measured electrically, in: Proceedings of the National Academy of Sciences, 88.17, 1991, pp. 7896–7900.
[12] I. Giaever, C.R. Keese, Fractal motion of mammalian cells, in: Physica D: Nonlinear Phenomena, vol. 38, 1989, pp. 128–133, 1-3.
[13] Fabián Eduardo Giana, Desarrollo de una técnica basada en mediciones de impedancia eléctrica para la discriminación in vitro entre células cancerosas y no cancerosas, PhD thesis, Universidad Nacional de Uncyo, Instituto Balseiro CONICET, 2018.
[14] Charles R. Gaush, L Hard Walter, Thomas F. Smith, Characterization of an established line of canine kidney cells (MDCK), in: Proceedings of the Society for Experimental Biology and Medicine, 122.3, 1966, pp. 931–935.
[15] M. Cereijido, et al., Fluxes, junctions, and blisters in cultured monolayers of epithelioid cells (MDCK), in: Annals of the New York Academy of Sciences, 372.1, 1981, pp. 422–441.
[16] C.R. Keese, C. Lo, I. Giaever, Impedance analysis of MDCK cells measured by electric cell-substrate impedance sensing, in: Biophysical Journal, 69.6, 1995, pp. 2800–2807.
[17] R Ian Freshney, Culture of Animal Cells: a Manual of Basic Technique and Specialized Applications, John Wiley & Sons, 2015.
[18] S Izzard Colin, R Lochner Linda, Formation of cell-to-substrate contacts during fibroblast motility: an interference-reflexion study, in: Journal of Cell Science, 42.1, 1980, pp. 81–116.
[19] Chun-Min Lo, Charles R. Keese, Ivar Giaever, Monitoring motion of confluent cells in tissue culture, in: Experimental Cell Research, 204.1, 1993, pp. 102–109.
[20] Tomoyuki Higuchi, Approach to an irregular time series on the basis of the fractal theory, in: Physica D: Nonlinear Phenomena, 31.2, 1988, pp. 277–283.
[21] A. Anier, et al., Higuchi fractal dimension and spectral entropy as measures of depth of sedation in intensive care units, in: The 26th Annual International Conference of the IEEE Engineering in Medicine and Biology Society, vol. 1, IEEE, 2004, pp. 526–529.
[22] Sou Nobukawa, et al., Atypical temporal-scalespecific fractal changes in Alzheimer's disease EEG and their relevance to cognitive decline, in: Cognitive Neurodynamics, 13.1, 2019, pp. 1–11.
[23] B.S. Raghavendra, Narayana D Dutt, Computing fractal dimension of signals using multiresolution box-counting method, in: International Journal of Information and Mathematical Sciences, 6.1, 2010, pp. 50–65.
[24] E. Fernandez, et al., Are neurons multifractals?, in: Journal of Neuroscience Methods, 89.2, 1999, pp. 151–157.
[25] Jens Feder, The Fractal Dimension, Springer, 1988, pp. 149–162.
[26] E.H. Lloyd, Long-Term Storage: an Experimental Study, Wiley Online Library, 1966.
[27] Herbert F. Jelinek, Eduardo Fernandez, Neurons and fractals: how reliable and useful are calculations of fractal dimensions?, in: Journal of Neuroscience Methods, vol. 81, 1998, pp. 9–18, 1-2.
[28] Omar Abu Arqub, Zaer Abo-Hammour, Numerical solution of systems of secondorder boundary value problems using continuous genetic algorithm, in: Information Sciences, 2014.
[29] Zaer Abo-Hammour, et al., Optimization solution of Troesch's and Bratu's problems of ordinary type using novel continuous genetic algorithm, in: Discrete Dynamics in Nature and Society, 2014.
[30] Dmitry Mottl, Hurst, 2019. https://github.com/Mottl/hurst.
[31] Charles R. Keese, et al., Electrical wound-healing assay for cells in vitro, in: Proceedings of the National Academy of Sciences, 101.6, 2004, pp. 1554–1559.
[32] Nazareno Gonz´alez, et al., Computational and in vitro pharmacodynamics characterization of 1A116 Rac1 inhibitor: relevance of Trp56 in its biological activity, in: Frontiers in Cell and Developmental Biology, vol. 8, 2020, p. 240.